

REPORT

The activity of Sac1 across ER–TGN contact sites requires the four-phosphate-adaptor-protein-1

Rossella Venditti^{1,2*}, Maria Chiara Masone^{1*}, Laura Rita Rega¹, Giuseppe Di Tullio¹, Michele Santoro¹, Elena Polishchuk¹, Ivan Castello Serrano¹, Vesa M. Olkkonen^{3,4}, Akihiro Harada⁵, Diego L. Medina¹, Raffaele La Montagna¹, and Maria Antonietta De Matteis^{1,2}

Phosphatidylinositol-4-phosphate (PI4P), a phosphoinositide with key roles in the Golgi complex, is made by Golgi-associated phosphatidylinositol-4 kinases and consumed by the 4-phosphatase Sac1 that, instead, is an ER membrane protein. Here, we show that the contact sites between the ER and the TGN (ERTGoCS) provide a spatial setting suitable for Sac1 to dephosphorylate PI4P at the TGN. The ERTGoCS, though necessary, are not sufficient for the phosphatase activity of Sac1 on TGN PI4P, since this needs the phosphatidyl-four-phosphate-adaptor-protein-1 (FAPP1). FAPP1 localizes at ERTGoCS, interacts with Sac1, and promotes its in-trans phosphatase activity in vitro. We envision that FAPP1, acting as a PI4P detector and adaptor, positions Sac1 close to TGN domains with elevated PI4P concentrations allowing PI4P consumption. Indeed, FAPP1 depletion induces an increase in TGN PI4P that leads to increased secretion of selected cargoes (e.g., ApoB100), indicating that FAPP1, by controlling PI4P levels, acts as a gatekeeper of Golgi exit.

Introduction

Phosphatidylinositol-4-phosphate (PI4P) is a phosphoinositide that has a pivotal role at the Golgi, in particular at the TGN, where it is enriched (Balla, 2013; De Matteis et al., 2013). PI4P mediates the association of adaptor proteins involved in cargo sorting, recruits components involved in carrier budding and fission, and drives sphingolipid synthesis and cholesterol transfer from the ER to the TGN (Hanada et al., 2003; Godi et al., 2004; D'Angelo et al., 2007, 2008; Valente et al., 2012; Mesmin et al., 2013). The steady-state levels of PI4P at the TGN are maintained by two phosphatidylinositol-4 kinases (PI4Ks; PI4KIII β and PI4KII α) and one 4-phosphatase (Sac1). While the PI4Ks are cytosolic proteins associated with the Golgi complex (Balla, 2013), Sac1 is an integral membrane protein that resides in the ER and cycles between the ER and early Golgi compartments (without reaching the TGN) in normally growing cells (Cheong et al., 2010) through COPII- and COPI-mediated anterograde and retrograde trafficking, respectively (Rohde et al., 2003; Bajaj Pahuja et al., 2015). One way for Sac1 to gain access to PI4P in the TGN could be to exploit the ER–TGN contact sites (ERTGoCS; Hsu and Mao, 2015). However, the gaps in our knowledge about ERTGoCS, mainly due to methodological limits, have hampered direct studies to address this question. We therefore developed a Förster resonance energy transfer-based approach (Grecco and Bastiaens, 2013), which is endowed with the necessary nanoscale resolution power for the

study of ERTGoCS that enabled us to identify some of the components required to establish/maintain the contacts (see Venditti et al. in this issue). These include the ER resident proteins VAPA and VAPB; the lipid transfer protein ORP10 which transfers PS; and OSBP1 and ORP9, which transfer cholesterol and play a redundant role in the maintenance of the ERTGoCS.

Here, we exploited the knowledge gained on the molecular requirements for ERTGoCS to address the question of whether and how they control the levels of PI4P at the TGN.

Results and discussion

Destabilizing the ERTGoCS increases PI4P levels at the TGN

To assess the role of ERTGoCS in controlling PI4P at the TGN, we evaluated what happens to TGN PI4P levels after depletion of the very same set of proteins we had tested for their effects on ERTGoCS, i.e., the VAP proteins (VAPA and VAPB) and the lipid transfer proteins that are associated with the Golgi complex (OSBP1, ORP9, ORP10, ORP11, CERT, FAPP1, and FAPP2).

We have shown (Venditti et al., 2019) that either depleting VAP proteins or ORP10, or the combined depletion of ORP9 and OSBP1, are the only conditions that destabilize ERTGoCS. Analyzing the levels of PI4P at the TGN by immunostaining, we observed that, in general, there is a very good correlation between

¹Telethon Institute of Genetics and Medicine, Pozzuoli, Italy; ²Department of Molecular Medicine and Medical Biotechnology, University of Napoli Federico II, Medical School, Naples, Italy; ³Minerva Foundation Institute for Medical Research, Biomedicum 2U, Helsinki, Finland; ⁴Department of Anatomy, Faculty of Medicine, University of Helsinki, Helsinki, Finland; ⁵Osaka University, Osaka, Japan.

*R. Venditti and M.C. Masone contributed equally to this paper; Correspondence to Maria Antonietta De Matteis: dematteis@tigem.it.

© 2019 Venditti et al. This article is distributed under the terms of an Attribution–Noncommercial–Share Alike–No Mirror Sites license for the first six months after the publication date (see <http://www.rupress.org/terms/>). After six months it is available under a Creative Commons License (Attribution–Noncommercial–Share Alike 4.0 International license, as described at <https://creativecommons.org/licenses/by-nc-sa/4.0/>).

conditions that induce the destabilization of ERTGoCS (Fig. 4 in Venditti et al., 2019) and those that cause an increase in PI4P levels at the TGN (Fig. 1, A–C). Indeed, only VAP depletion, ORP10 depletion, and the combined depletion of OSBP1 and ORP9 led to increased levels of PI4P at the TGN, indicating that the close proximity of ER and TGN membranes is a prerequisite for Sac1 to dephosphorylate Golgi PI4P (Fig. 1, A–C).

FAPP1 depletion causes an increase in Golgi PI4P without affecting the stability of the ERTGoCS

One notable exception to the general correlation between ERTGoCS destabilization and the increase in Golgi PI4P was FAPP1, whose depletion had no effect on the number or integrity of ERTGoCS (Fig. 4 in Venditti et al., 2019) but markedly increased Golgi PI4P levels (Fig. 1, A, B, and D). The increase in Golgi PI4P levels was evaluated by four independent approaches: three imaging approaches and a biochemical one. The imaging approaches were based on the use of an anti-PI4P antibody (Hammond et al., 2009; Fig. 1, A–D), on the expression of two different genetically encoded PI4P probes (P4C and P4M; Hammond et al., 2014; Luo et al., 2015; Fig. 1, E and F; and Fig. S1, A and B), and on the staining of permeabilized cells with a recombinant PI4P probe (the PH domain of FAPP1; Godi et al., 2004; Fig. S1 C). The biochemical approach was based on a mass assay in which Golgi fractions were incubated with recombinant PI4P 5-kinase type-1 γ (PIP5K1C) and $[\gamma\text{-}^{32}\text{P}]\text{-ATP}$. The amount of ^{32}P -PI4,5P₂ generated under these conditions and assessed by TLC is a measure of the PI4P 5-kinase substrate (i.e., PI4P) present in the membranes. A higher amount of PI4,5P₂ was produced by PIP5K1C incubated with Golgi fractions isolated from FAPP1-depleted cells as compared with control cells (Fig. 1, G and H), confirming that FAPP1 depletion increases Golgi PI4P.

Importantly, the effect of FAPP1 depletion on PI4P was rescued by the expression of siRNA-resistant forms of FAPP1 (Fig. 1D) and, more importantly, fibroblasts from FAPP1-KO mice exhibited an increase in PI4P levels in the Golgi (in comparison to control fibroblasts) that was reverted by the expression of human FAPP1 (Figs. 1D and S1 D). These results indicated that the balance of PI4P at the Golgi requires ERTGoCS integrity and functional FAPP1.

FAPP1 interacts with VAPs and Sac1

FAPP1, encoded by the *PLEKHA3* gene, was among the first mammalian PI4P-binding proteins to be identified (Dowler et al., 2000), but its role has remained elusive so far (D'Angelo et al., 2007; De Matteis et al., 2007). Our observation that FAPP1 controls PI4P levels at the Golgi, but not the integrity of ERTGoCS, prompted us to investigate the molecular mechanisms underlying this control. We combined proximity-biotinylation (Fig. 2A), coimmunoprecipitation (Fig. S2, A and B), and in vitro binding assays with recombinant proteins (Fig. 2, B and C) to look for and validate FAPP1 interactors and found that FAPP1 interacts directly and forms a tripartite complex with VAP proteins and Sac1 (Fig. 2, A–C). We dissected the domains of FAPP1 involved in these interactions and found that it binds the N-terminal regulatory domain of Sac1 via its N-terminal domain and VAPA via its C-terminal region (Fig. 2, B and C).

The interaction of FAPP1, a TGN-associated protein, with two ER proteins (VAP and Sac1) prompted us to investigate whether FAPP1 localizes at ERTGoCS and whether the interaction of FAPP1 with Sac1 had any impact on the phosphatase activity of Sac1. Using super-resolution microscopy and immuno-EM, we were able to visualize FAPP1 at sites of apposition of the TGN with the ER (Fig. 2, D and E).

FAPP1 promotes the in-trans phosphatase activity of Sac1

We then assessed whether FAPP1 could affect the 4-phosphatase activity of Sac1. This was tested in vitro using recombinant human proteins (Sac1 and FAPP1) and reconstituting different configurations of enzyme–substrate interaction (cis, trans, or soluble forms of the substrate). We found that the in-trans phosphatase activity of Sac1 is rather low, in agreement with previous reports obtained with yeast Sac1 (Mesmin et al., 2013), but is markedly stimulated by FAPP1 in a dose-dependent manner (Fig. 2, F and H). Intriguingly, FAPP1 behaved as a powerful activator of the dephosphorylation of PI4P by Sac1 in trans, while it had a much smaller effect on the dephosphorylation of PI4P in cis and no effect on the dephosphorylation of a soluble form of PI4P by Sac1 (Fig. 2, F and G). We asked whether FAPP1 could “present” PI4P to Sac1, in which case it should be able to extract PI4P from membranes, but found that this was not the case (Fig. 2 I). We also checked whether the Sac1 dephosphorylation of PI4P that is stimulated by FAPP1 might be due to a possible liposome aggregation activity of FAPP1. This was not the case since FAPP1 exhibited no liposome aggregation activity at concentrations that were effective in stimulating Sac1 phosphatase activity. Slight liposome aggregation was observed only with the highest concentrations of FAPP1, which, however, stimulated Sac1 activity 10-fold more than an artificial tether, inducing comparable levels of liposome aggregation (Fig. S2, C and D).

Increasing the stability of ERTGoCs decreases Golgi PI4P in a FAPP1-dependent manner

The above results indicate that FAPP1 activates the in-trans activity of Sac1 in vitro. We then assessed whether this could also occur in cells. To this end we developed an optogenetics approach to stabilize ERTGoCS in a reversible manner and to simultaneously follow the levels of PI4P. The light-oxygen-voltage (LOV)-sensitive domain of phototropin was fused to SsrA and the ER reporter domain (Cb5), while the reciprocal peptide Sspb was fused to the TGN reporter protein (TGN46; Lungu et al., 2012; Guntas et al., 2015; Fig. 3, A and B). In the absence of illumination, Cb5 had a diffuse ER distribution but concentrated around the Golgi area after blue light illumination. This concentration was lost when the blue light was removed (Fig. 3 C and Video 1). The simultaneous detection of PI4P levels by the PI4P probe P4M (Hammond et al., 2014) in living cells (Fig. 3, C and D; and Video 1) or by the anti-PI4P antibody (Hammond et al., 2009) in fixed cells (Fig. 3, E and F) showed an anti-phasic trend, with the levels of TGN PI4P decreasing in coincidence with the increased stability of the ERTGoCS (Fig. 3, D–F; and Video 1). Importantly, this decrease was dependent on FAPP1, as it was blunted in FAPP1-depleted cells (Fig. 3 D).

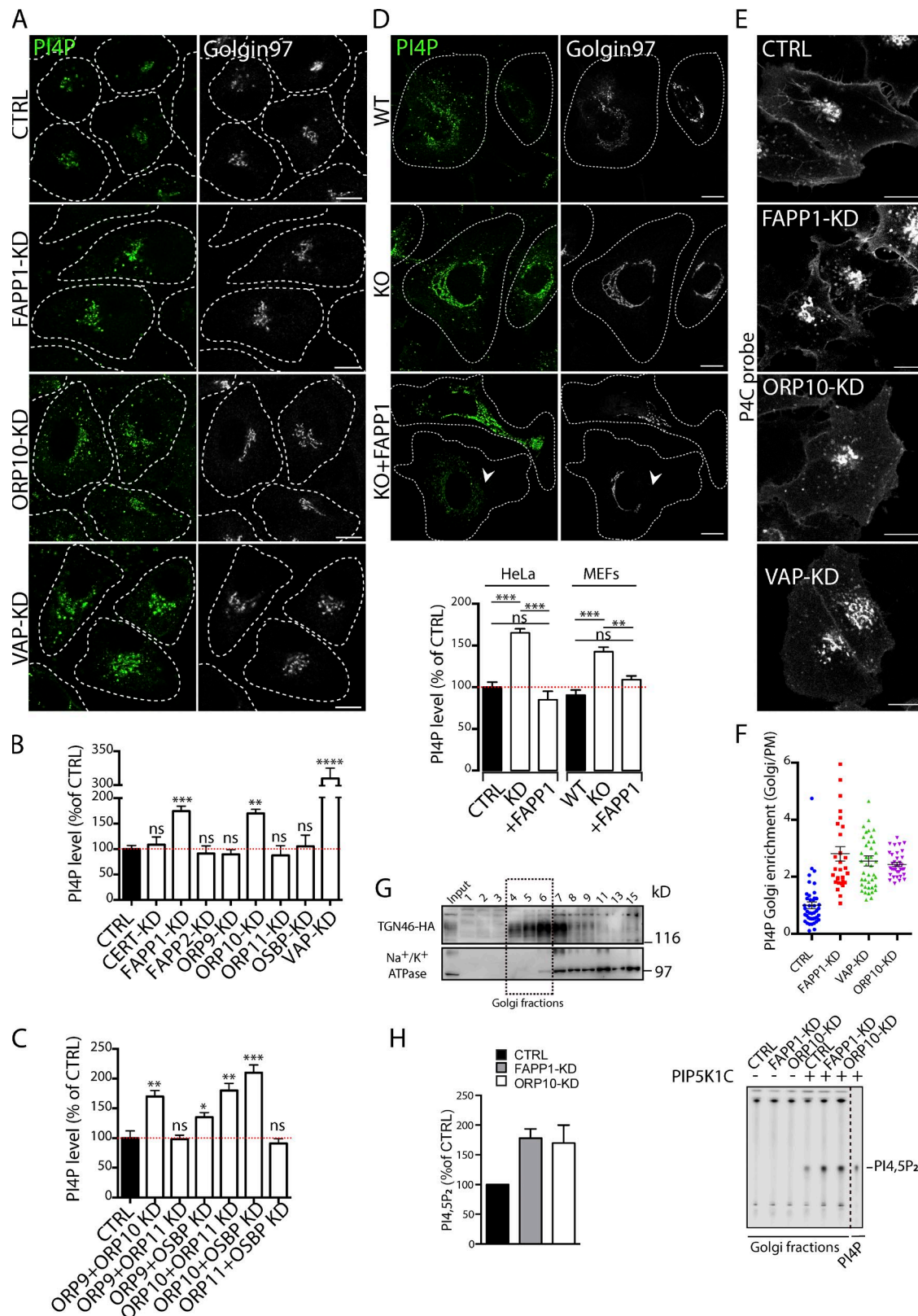


Figure 1. The depletion of VAPs, ORP10, and ORP9 in combination with OSBP1, or of FAPP1 increases Golgi PI4P. (A) Immunodetection of PI4P with a monoclonal anti-PI4P antibody in control (CTRL), FAPP1-KD, ORP10-KD, and VAP-KD HeLa cells fixed and costained with anti-Golgin-97 antibody. Bar, 10 μ m. (B and C) Quantification of Golgi PI4P levels (the ratio of PI4P and Golgin-97 fluorescence intensity at the Golgi complex; see Materials and methods) in cells transfected with the indicated single (B) or double (C) siRNAs. Means \pm SD, three independent experiments, $n > 200$ cells per experiment; Student's t test. Bar, 10 μ m. (D) PI4P levels in control and FAPP1-KD HeLa cells and in WT and FAPP1-KO MEFs with (+FAPP1) or without GFP-FAPP1 overexpression. Top panel: Representative images of the MEFs. The arrowhead in a lower panel indicates a cell overexpressing GFP-FAPP1. Graph: Quantification of Golgi PI4P levels

In a parallel approach, we stabilized ERTGoCS, using rapamycin to induce the heterodimerization of the ER and TGN reporter proteins containing the FKBP and FRB domains, respectively (Fig. 3, G and H). The stabilization of ERTGoCS induced by rapamycin resulted in a decrease in PI4P levels, which was faster and more pronounced than that induced by the optogenetics-based stabilization (Fig. 3 E), possibly due to the different geometries, efficiency, and stability of the induced dimers.

The levels of TGN PI4P were reduced by 60% and by 80% upon 2–4-min and 15-min treatments with rapamycin in control cells, respectively (Fig. 3, I and J). The decrease in PI4P levels was less pronounced in FAPP1-depleted cells, consistent with the involvement of FAPP1 in controlling the phosphatase activity of Sac1 (Fig. 3, I and J). The observed decrease of Golgi PI4P induced by ERTGoCS stabilization in FAPP1-depleted cells may be due to a residual fraction of FAPP1 or to a FAPP1-independent in-trans activity of Sac1 under conditions of forced stabilization of the ERTGoCS, or, to an in-cis activity of Sac1 sustained by the transfer of PI4P from the TGN to the ER via the lipid transfer proteins OSBP1 and/or ORP9 (Ngo and Ridgway, 2009; Mesmin et al., 2013). We thus applied the above ERTGoCS-stabilizing treatments to conditions, such as VAP depletion (by siRNA or transcription activator–like effector nuclease [TALEN]), that prevent TGN-to-ER transfer of PI4P by OSBP1 or ORP9 (as VAPs are the necessary ER anchors for these lipid transfer proteins; Murphy and Levine, 2016).

Under these conditions, the TGN PI4P has to be obligatorily consumed in trans by Sac1. We first checked the ability of the treatments to stabilize the ERTGoCS. While short treatments (2–4 min) with rapamycin, which induced stabilization of ERTGoCS in control cells, were ineffective in VAP-depleted cells, longer rapamycin treatment (15 min) could induce a significant stabilization of ERTGoCS even in VAP-depleted cells (Fig. 3, I–K). Of note, the 15-min treatment (but not the 2–4-min treatments) could also reduce the elevated PI4P levels in VAP-depleted cells (Fig. 3, I–K), but only in the presence of FAPP1, since the stabilization of the ERTGoCS in cells depleted both for VAPs and FAPP1 had no effect on the elevated PI4P levels in these cells (Fig. 3, I and J), in line with the requirement of FAPP1 for the in-trans 4-phosphatase activity of Sac1, and also with the observation that FAPP1, at least in vitro, can promote the in-trans activity of Sac1 in the absence of VAPs (Fig. 2, F and H).

FAPP1 negatively controls the secretion of ApoB100 in hepatocytes by titrating PI4P levels at the TGN

Having uncovered a role for FAPP1 as a controller of PI4P at the TGN, we wondered about the functional relevance of such a role.

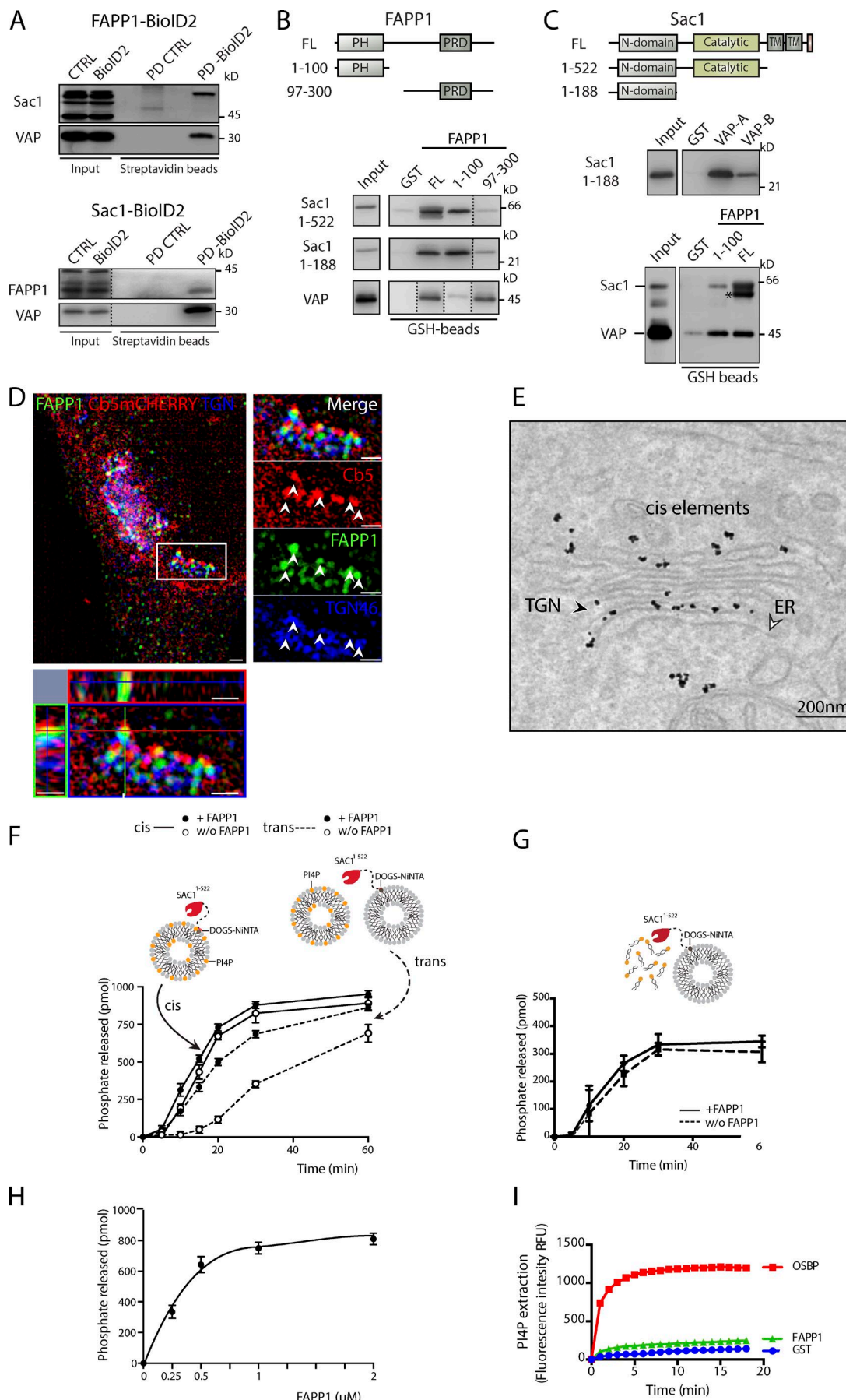
In addressing this question, we were guided by the reported observation that the depletion of ORP10, which leads to an increase in Golgi PI4P analogous to that induced by FAPP1 depletion (Fig. 1, A and B), stimulates the secretion of ApoB100, but not of albumin, in hepatocytes (Nissilä et al., 2012). Interestingly, the role of ORP10 as a negative controller of ApoB100 secretion has been proposed as a possible explanation for the association of ORP10 single-nucleotide polymorphisms with dyslipidemia and peripheral arterial disease (Perttälä et al., 2009; Koriyama et al., 2010; Nissilä et al., 2012). Thus, we assessed the role of FAPP1 in ApoB100 secretion. We found that FAPP1 and ORP10 act as negative regulators of TGN PI4P and that FAPP1, like ORP10, negatively regulates ApoB100 secretion in HepG2 cells (Fig. 4, A–E). Indeed, the depletion of FAPP1 induced an increase in the secretion of ApoB100, as evaluated by Western blot (Fig. 4, A and B), ELISA (Fig. 4 C), and pulse-chase analysis of newly synthesized ApoB100 (Fig. 4 D), while it did not affect the secretion of other newly synthesized cargoes, such as albumin and α 1-antitrypsin (Fig. 4 D).

To identify the trafficking step of ApoB100 that is sensitive to FAPP1 regulation, we devised a synchronization protocol whereby newly synthesized ApoB100 was first accumulated in the TGN (by lowering the temperature to 20°C) and then allowed to exit the TGN by increasing the temperature to 37°C. We found that FAPP1 depletion accelerates the exit of ApoB100 from the TGN (Fig. 4, G and H) and increased the number of post-Golgi carriers containing ApoB100 (Fig. 4 I). Importantly, the accelerated Golgi-emptying of ApoB100 was blunted by the simultaneous depletion of PI4KIII β , indicating that it was due to increased PI4P levels (Fig. 4 H). The above data indicate that FAPP1 titrates PI4P to levels that limit the rate of transport of selected cargoes, such as ApoB100, which use dedicated carriers to leave the TGN (Hossain et al., 2014).

Here, we have identified that FAPP1, a protein with an enigmatic function so far (D'Angelo et al., 2007; De Matteis et al., 2007), is a regulator of Golgi PI4P levels, which can activate the in-trans 4-phosphatase activity of Sac1. We envisage that FAPP1, faithful to its original name of phosphatidyl-four-phosphate-adaptor-protein-1 (Dowler et al., 2000), acts as an adaptor between PI4P-enriched TGN domains and Sac1 in the ER membranes, boosting, but at the same time restricting in space, its phosphatase activity across the ERTGoCS. In yeast, targeting the activity of Sac1 toward a specific pool of PI4P (in the early Golgi compartments) has been proposed for Vps74 (Wood et al., 2012).

Sac1 can also act in cis on PI4P that is transferred from the TGN to the ER by OSBP1 in counter-exchange with cholesterol (Mesmin et al., 2013). We believe that the two modes of Sac1 activity coexist

in control and FAPP1-KD HeLa cells and in WT and FAPP1-KO MEFs, with (+FAPP1) or without GFP-FAPP1 overexpression. Means \pm SD, three independent experiments, $n = 60$ –80 cells per experiment. *, $P < 0.05$; **, $P < 0.01$; ***, $P < 0.001$; ****, $P < 0.0001$ in B–D; Student's t test. (E) Distribution of the PI4P GFP-P4C probe in control, FAPP1-KD, ORP10-KD, and VAP-KD fixed HeLa cells. Bar, 10 μ m. (F) The ratio between GFP-P4C fluorescence intensity in the Golgi and PM area. Means \pm SD, three independent experiments, $n = 30$ –43 cells/condition. (G and H) Evaluation of Golgi PI4P levels by mass assay. (G) Golgi fractions were isolated from control (CTRL), FAPP1-KD, and ORP10-KD HeLa cells (see Materials and methods). Western blot showing the distribution of a TGN protein (TGN46) and a PM protein (Na⁺/K⁺ ATPase) after sucrose gradient separation. Dashed rectangle, fractions enriched for Golgi markers. (H) Golgi fractions were incubated with ³²P-ATP and, where indicated, with recombinant PIP5K1C. ³²P-PI4,5P₂ produced by PIP5K1C incubated with 3 μ M porcine brain PI4P (PI4P, right lane) was taken as a reference for PI4,5P₂. The amount of ³²P-PI4,5P₂ produced by PIP5K1C using PI4P present in Golgi fractions as a substrate was assessed by TLC and expressed as a percentage of control (graph). Means \pm SD of three independent experiments.



with different physical constraints and possibly distinct but integrated functions (Fig. 5). Given that the width of ERTGoCS ranges from 5 to 20 nm (Venditti et al., 2019), the in-trans activity of Sac1 may occur only at the tighter contact sites and only when FAPP1 is present. These sites, considering the low affinity of FAPP1 for PI4P (K_d : 18.6 μ M; Levine and Munro, 2002), should also have initially elevated PI4P concentrations. In this way, FAPP1 acts at the same time as a PI4P detector and as an activator of Sac1, thus emerging as a pivotal regulator of the PI4P levels in the TGN and hence of PI4P-dependent physiological or pathological Golgi-based processes (Balla, 2013; De Matteis et al., 2013). In the in-cis mode, Sac1 acts on the PI4P pool that is transferred from the TGN to the ER by OSBP1. In this mode, Sac1 can operate also at contact sites that have a greater distance between the opposing membranes since OSBP1 can in principle shuttle between the TGN and the ER (Fig. 5 A).

We propose that the paradigm of coexisting modes of Sac1 activity at membrane contact sites might be extended to the plasma membrane (PM)–ER and endosome–ER contact sites where Sac1 also patrols local pools of PI4P (Chung et al., 2015; Dickson et al., 2016; Dong et al., 2016; Sohn et al., 2018; Zewe et al., 2018). While the requirements for the in-cis activity of Sac1 at the PM–ER and endosome–ER contact sites have been identified (Chung et al., 2015; Dong et al., 2016; Sohn et al., 2018; Zewe et al., 2018), the possibility that FAPP1-like factors could act locally as activators of the in-trans activity of Sac1 on PM or endosomal PI4P has not been explored, with the exception of Osh3, which, in yeast, has been shown to be required for Sac1 activity on PM PI4P independently of its lipid transfer activity (Stefan et al., 2011). We anticipate that our findings on FAPP1 activity at the ERTGoCS will foster the search for activators of the in-trans activity of Sac1 at other contact sites in mammalian cells.

Finally, we shed light on the physiological relevance of the role we have uncovered for FAPP1 and ERTGoCS as controllers of Golgi PI4P. By allowing the consumption of PI4P at the ERTGoCS, FAPP1 exerts a negative control on PI4P levels and, as we have shown, on ApoB100 secretion. This finding reveals an unpredicted function for ERTGoCS. To date, membrane contacts have been regarded as structures that have a permissive/positive role in membrane remodeling events (Phillips and Voeltz, 2016; Caldieri et al., 2017). Here, we have provided an example of membrane contacts acting as negative controllers of selected carrier budding at the TGN

via their control of PI4P levels. Since only a fraction of the Golgi stacks is engaged in ERTGoCS (Venditti et al., 2019), one could envisage two possible scenarios: either the TGN of all the stacks has equivalent PI4P, in which case each Golgi stack engages in transient contacts with the ER, or the TGN of different stacks have heterogeneous PI4P content, in which case only a subset of Golgi stacks engages in stable contacts with the ER while the remainder do not. Further, considering that ERTGoCS, by controlling PI4P levels, can negatively regulate the TGN export of ApoB100, one can envision that every stack can export ApoB100 at a low rate or that stacks with high rates of ApoB100 export coexist with stacks that do not export ApoB100 (Fig. 5 B). Resolving these issues will require a high-resolution map of PI4P distribution and of ApoB100 carrier budding at the TGN.

Materials and methods

Reagents and antibodies

Primary antibodies used in this study were mouse monoclonal anti-HA and rabbit polyclonal anti-HA (Covance), mouse monoclonal anti-PI4P (Echelon), mouse monoclonal anti-His (Qiagen), rabbit polyclonal anti-Sac1 (Proteintech), rabbit polyclonal anti-ORP9 (Sigma-Aldrich), rabbit polyclonal anti-ORP10 (Pierce), rabbit polyclonal anti- β -actin (Sigma-Aldrich), sheep polyclonal anti-TGN46 (Serotec), mouse monoclonal anti- Na^+/K^+ ATPase (Cell Signaling), and mouse monoclonal anti-Giantin (Abcam). Rabbit polyclonal antibodies against FAPP1, FAPP2, VAP-A, VAP-B, GST (Venditti et al., 2012), Golgin-97, and ORP11 and rabbit polyclonal antibodies raised against full-length (FL) CERT and OSBP1 were obtained in our laboratories as described in Venditti et al. (2019). 1,2-dioleoyl-*sn*-glycero-3-phosphocholine (DOPC), 1,2-dioleoyl-*sn*-glycero-3-phosphoethanolamine (DOPE), 1,2-dioleoyl-*sn*-glycero-3-phospho-L-serine (DOPS), 1,2-dioleoyl-*sn*-glycerol-3-[(N-(5-amino-1-carboxypentyl) iminodiacetic acid)succinyl] (DOGS-NTA-Ni; nickel salt), TopFluor-PI4P, and porcine brain PI4P were purchased from Avanti Polar Lipids. diC8-PI4P was purchased from Echelon Biosciences. DiIC18 was purchased from Thermo Fisher Scientific. Recombinant PIP5K1C was purchased from ProQinase.

The following reagents were gifts: pSPORT6-hSac1 and GFP-P4M, from T. Balla (National Institutes of Health, Bethesda,

Figure 2. FAPP1 interacts with VAPs and Sac1 and promotes the in-trans 4-phosphatase activity of Sac1 in vitro. (A) HeLa cells transfected with FAPP1-BioID2 or Sac1-BioID2 constructs were treated with 50 μ M biotin. Biotinylated proteins were used in a PD assay with streptavidin-conjugated beads, resolved by SDS-PAGE, and immunoblotted with the indicated antibodies. (B) In vitro PD of GST-FAPP1 proteins (FL, residues 1–100, or residues 97–300) with His-tagged forms of Sac1 and VAPA showing direct binding to Sac1 (residues 1–522 and 1–188) and to VAPA. (C) Top: In vitro PD of His-Sac1 (residues 1–188) with GST-tagged VAPA and VAPB proteins. Bottom: GST-FAPP1 PD assay shows simultaneous binding with Sac1 (1–522) and VAPA. The asterisk indicates cross-reaction of the anti-His-antibody with FL-FAPP1. (D) SIM–super resolution images of endogenous FAPP1 localizing at ERTGoCS. Right panels: Magnification of boxed area; arrowheads indicate interposition of FAPP1 (green) between the TGN (TGN46 in blue) and the ER (Cb5 in red), as highlighted in the orthogonal projection (bottom). Bars, 1 μ m. (E) Immuno-EM image showing FAPP1 localizing at the ERTGoCS. FAPP1 was enriched at the TGN as compared with earlier Golgi compartments, as previously described (Godi et al., 2004). (F) In vitro 4-phosphatase activity of liposome-bound His6-Sac1 (1–522) in the presence of GST-FAPP1 (+FAPP1) or GST alone (without FAPP1) in the cis (solid line) or trans (dotted line) conformation (schematized above panel). The reaction was performed in 100 μ l in the presence of 100 nM Sac1; 12.5 μ l was taken at the indicated time points to measure phosphate release (see Materials and methods). Means \pm SD, three technical replicates of a representative experiment, $n = 3$. (G) Effects of GST-FAPP1 or GST alone (w/o FAPP1) on liposome-bound His6-Sac1 (1–522) activity toward soluble diC8-PI4P. Means \pm SD, three technical replicates of a representative experiment, $n = 3$. (H) Dose response of phosphate release in the trans conformation in the presence of increasing concentrations of GST-FAPP1. Means \pm SD, three technical replicates of a representative experiment, $n = 3$ (see Materials and methods for details). (I) OSBP1 but not FAPP1 can extract PI4P from membranes. 3 μ M GST-OSBP1-FL (red line), GST-FAPP1-FL (green line) or GST (blue line) was added to liposomes containing TopFluor-PI4P and DiIC18 (see Materials and methods).

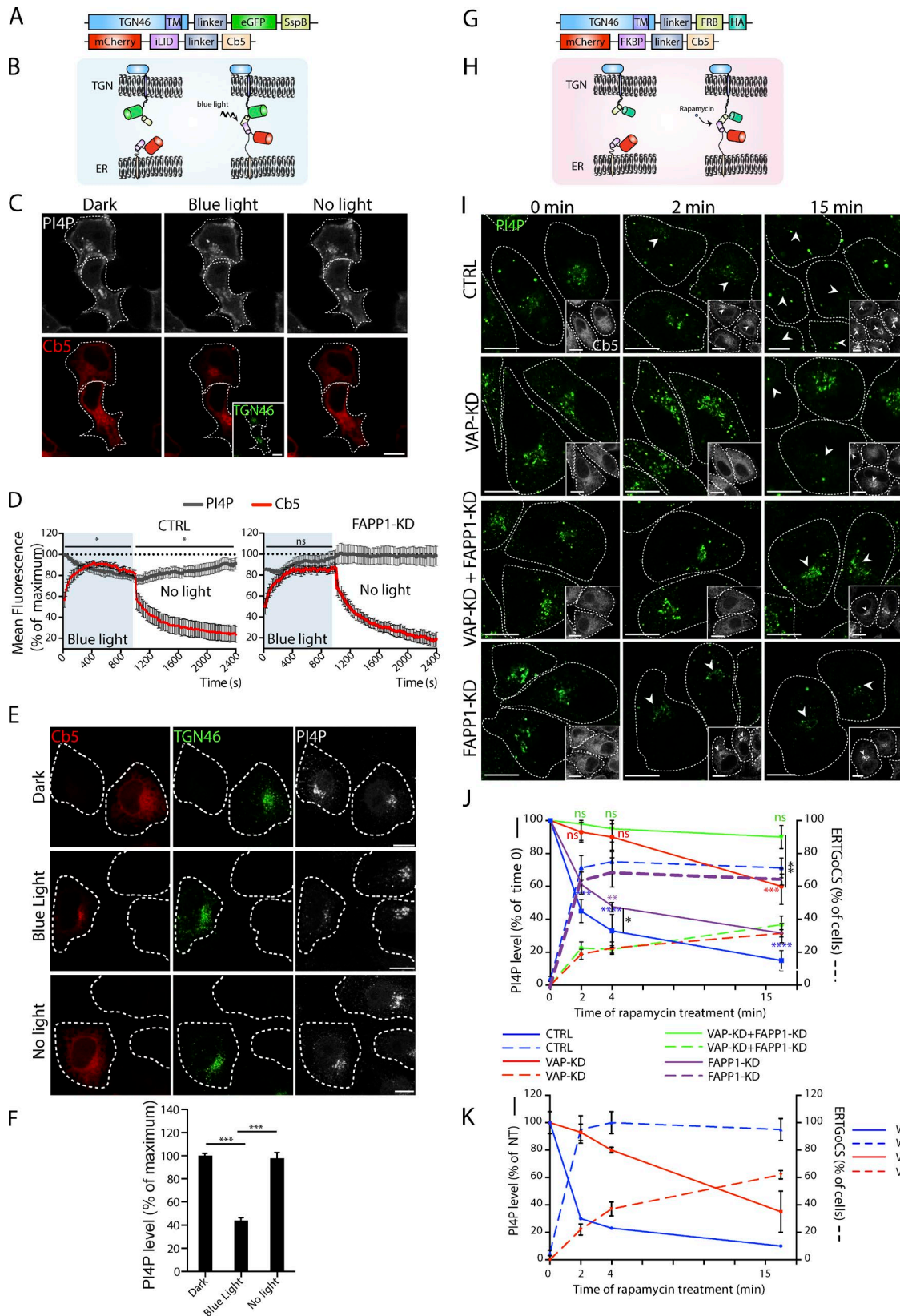


Figure 3. The stabilization of ERTGoCS decreases PI4P at the TGN in a FAPP1-dependent manner. (A) Schematic representation of the opto-ERTGoCS construct. (B) The optogenetic approach used to visualize ERTGoCS. In the absence of light (left), the ER-fused SsrA domain is enclosed in the C-terminal helix of the LOV domain (iLID construct). Blue light activation (488 nm, right) induces a conformational change that releases the SsrA domain, allowing its dimerization with the TGN-fused SspB domain and, in turn, ERTGoCS stabilization. (C) Representative images of HeLa cells transfected with the opto-ERTGoCS construct and with the PI4P probe P4M (PI4P). Cells were kept in the dark (left panels) and pulsed with blue light (488 nm; middle panels), and then the blue light was

MD); GFP-P4C from Y. Mao (Cornell University, Ithaca, NY); pcDNA3.1-VAPA and pGEX-VAPA from N. Ridgway (Atlantic Research Centre, Dalhousie University, Halifax, Nova Scotia, Canada). Other plasmids used were pGEX-4T2 from GE Healthcare; pTrcHis2 and Champion pET-SUMO from Thermo Fisher Scientific; and iRFP-P4M-SidM (51470), Myc-BioID2-MCS (74223), Venus-iLID-CAAX (60411), and tgRFPt-SspB WT (60415) from AddGene.

Media, serum, and reagents for tissue culture were purchased from Thermo Fisher Scientific. Unless otherwise stated, all chemicals were purchased from Sigma-Aldrich.

Plasmid construction

All reagents for molecular biology were purchased from New England Biolabs. All mutagenesis was performed by site-directed mutagenesis (Agilent Technologies). The ERTGoCS reporter construct TGN46-FRB-HA-GFP-T2A-mCherry-FKBP-Cb5-pIRES-neo2 was generated as described in Venditti et al. (2019).

The optogenetics control system to visualize ER-Golgi ERTGoCS is based on light-induced dimerization of the bacterial proteolysis tag peptide SsrA and its natural partner SspB with the ER reporter Cb5 and the TGN reporter TGN46, respectively. Without blue light stimulation (488 nm), the SsrA peptide is embedded in the C-terminal helix of the LOV domain. Upon photo-activation by illumination at 488 nm, the LOV helix unwinds, allowing the heterodimerization of SsrA and SspB (Lungu et al., 2012; Guntas et al., 2015).

To generate the optogenetics ERTGoCS (opto-ERTGoCS) reporter construct, the PIPE cloning strategy for multiple PCR assembly was used to clone GFP, SspB, T2A-mCherry, and iLID (LOV and SsrA peptide) genes (Table S1) using the TGN46-FRB-HA-GFP-T2A-mCherry-FKBP-Cb5-pIRES-neo2 as a template vector (replacing FRB-HA-GFP-T2A-mCherry-FKBP) to generate TGN46-GFP-SspB-T2A-mCherry-iLID-Cb5-pIRES-neo2.

All the cloning strategies adopted for generating the other plasmids used in this study are summarized in Table S1. The FAPP1, Sac1, VAP-A, and VAP-B plasmids refer to human sequences.

Cell culture, transfection, and RNA interference

HeLa cells and mouse embryonic fibroblasts (MEFs) were grown in high glucose (4,500 mg/l) DMEM supplemented with 10% FCS. HepG2 were grown in MEM supplemented with 1 mM sodium pyruvate, nonessential amino acids, and 10% FCS. HeLa WT and HeLa VAP-KO cell lines were a gift from P. De Camilli (Yale University School of Medicine, New Haven, CT). VAP-KO cells were generated by a TALEN-based gene-editing approach with TALEN pairs specific to exon 2 of VAPA and VAPB and were cultured as previously described (Dong et al., 2016). HeLa cells stably expressing the ERTGoCS pIRES-neo2 reporter and GFP-FAPP1 vectors were isolated as a clone obtained by single-cell-sorting procedures.

For transfection of DNA plasmids, HeLa cells were transfected using either TransIT-LT1 (Mirus Bio LLC, for BioID2 experiment) or JetPEI (Polyplus, for immunofluorescence analysis) as transfection reagents, and the expression was maintained for 16 h before processing.

The following siRNA sequences were used in this study. Cells treated with identical concentrations of non-targeting siRNAs (D-001810-01-20 and D-001810-02-20; Dharmacon) are referred to as controls. VAP-A: #1 5'-CACAGACCUCUAAAUA-3', #2 5'-GGC AAAACCUGAUGAAUUA-3', #3 5'-CCUGAGAGAUGAAGGUUA-3', #4 5'-CAAGGAAACUAAUGGAAGA-3'; VAP-B: #1 5'-GUAAGA GGCUGCAAGGUGA-3', #2 5'-CCACGUAGGUACUGUGUGA-3', #3 5'-UGUUACAGCCUUUCGAUUA-3', #4 5'-GUAUUUAUUGGGAAG AUUG-3'; FAPP1: #1 5'-CGAAGAACCUACUCAGAUUA-3', #2 5'-GCA UAAAGAUGGCAGUUUG-3', #3 5'-UCACAACGCUUGAGGAAUG-3', #4 5'-GAACCAGUAUCUACACUUC-3'; FAPP2: #1 5'-GAGAU A GACUGCAGCAUAU-3', #2 5'-GAAUUGAUGUGGGAACUUU-3', #3 5'-GAAAUCAACCUGUAAUACU-3', #4 5'-CCUAAAGAAAUCC AACAGAA-3'; OSBP1: #1 5'-CACAACUGUACACAACAUU-3', #2 5'-GAUAGAUCAGUCUGGCGAA-3'; ORP9: #1 5'-GAGGAGCACAAG AGCGUUA-3', #2 5'-ACCAAGAAGUUGCCUUAUA-3', #3 5'-GCU CAUAUCUGGACCAAAU-3', #4 5'-CCAAAGCGCUAAUAGAUU-3'; ORP10: #1 5'-CAACCCAAACCAACCAAUU-3', #2 5'-GGAUCA GCGUAGUAUAAUU-3', #3 5'-AAUACCACAUGGAAAUGAA-3'; ORP11: #1 5'-GAGACUUAUUAGACGAAU-3', #2 5'-GAAUCUGGA CUAUUAGCGA-3', #3 5'-GCGUGACAAUGGUUGGAGA-3'; CERT: #1 5'-GAAGAUGACUUUCCUACAA-3', #2 5'-GAAGUUGGCUGA

removed (right panels). After blue light stimulation, Cb5 is recruited to the TGN46-GFP area (inset, middle panels) and P4M Golgi localization is reduced. After removal of blue light, Cb5 returns to the ER localization, and P4M intensity increases in the Golgi area. Bar, 10 μ m. (D) Mean fluorescence intensity values \pm SD of Cb5-mCherry (red) and P4M (gray) in the Golgi area (defined as TGN46-GFP localization; see Materials and methods) in control (left) and in FAPP1-KD cells (right). *, $P < 0.05$. (E) mCherry-LOV-SsrA-Cb5 localization and PI4P Golgi levels (detected by anti-PI4P antibody) in HeLa cells transfected with the opto-ERTGoCS construct in the dark (top panels), exposed to a blue-light pulse (middle panels) and after removal of light stimulus (bottom panels). Bar, 10 μ m. (F) Quantification of the ratio of PI4P and Golgin-97 fluorescence intensity in the Golgi area expressed as a percentage of maximum. Three independent experiments, $n = 50$. ***, $P < 0.001$; Student's t test. (G and H) Schematic representation of constructs used to stabilize the ERTGoCS with rapamycin. (I) PI4P distribution in control, VAP-KD, FAPP1-KD, and VAP-KD+FAPP1-KD cells expressing TGN46-FRB-HA and mCherry-T2A-FKBP-Cb5 reporter proteins upon short (2 min rapamycin, middle panel) and prolonged (15 min rapamycin, right panel) stabilization of ERTGoCS. Inserts show Cb5 localization. Arrowheads indicate ERTGoCS formation. Bar, 10 μ m. (J) Quantification of Golgi PI4P levels (solid lines) and number of cells forming ERTGoCS (dashed lines) in control, VAP-KD, FAPP1-KD, and VAP-KD+FAPP1-KD cells treated with 200 nM rapamycin for the indicated times. PI4P was detected using a monoclonal anti-PI4P antibody, and PI4P levels were calculated as the ratio between PI4P and Golgin-97 fluorescence intensity at the Golgi complex. PI4P values are expressed as a percentage of values in cells at time 0 (not exposed to rapamycin). ERTGoCS values are expressed as a percentage of cells showing colocalization of Cb5 with TGN46. Means \pm SD, three independent experiments; $n = 60$ –100 cells. *, $P < 0.05$; **, $P < 0.01$; ***, $P < 0.001$; ****, $P < 0.0001$; Student's t test. (K) Golgi PI4P levels (solid lines) and number of cells forming ERTGoCS (dashed lines) in HeLa WT and VAP-KO cells treated with 200 nM rapamycin for the indicated times. PI4P levels were calculated as the ratio between PI4P and Golgin-97 fluorescence intensity at the Golgi complex. PI4P values are expressed as a percentage of values at time 0 (cells not exposed to rapamycin). ERTGoCS values are expressed as a percentage of cells showing colocalization of Cb5 with TGN46. Means \pm SD, three independent experiments; $n = 60$ –100 cells; Student's t test.

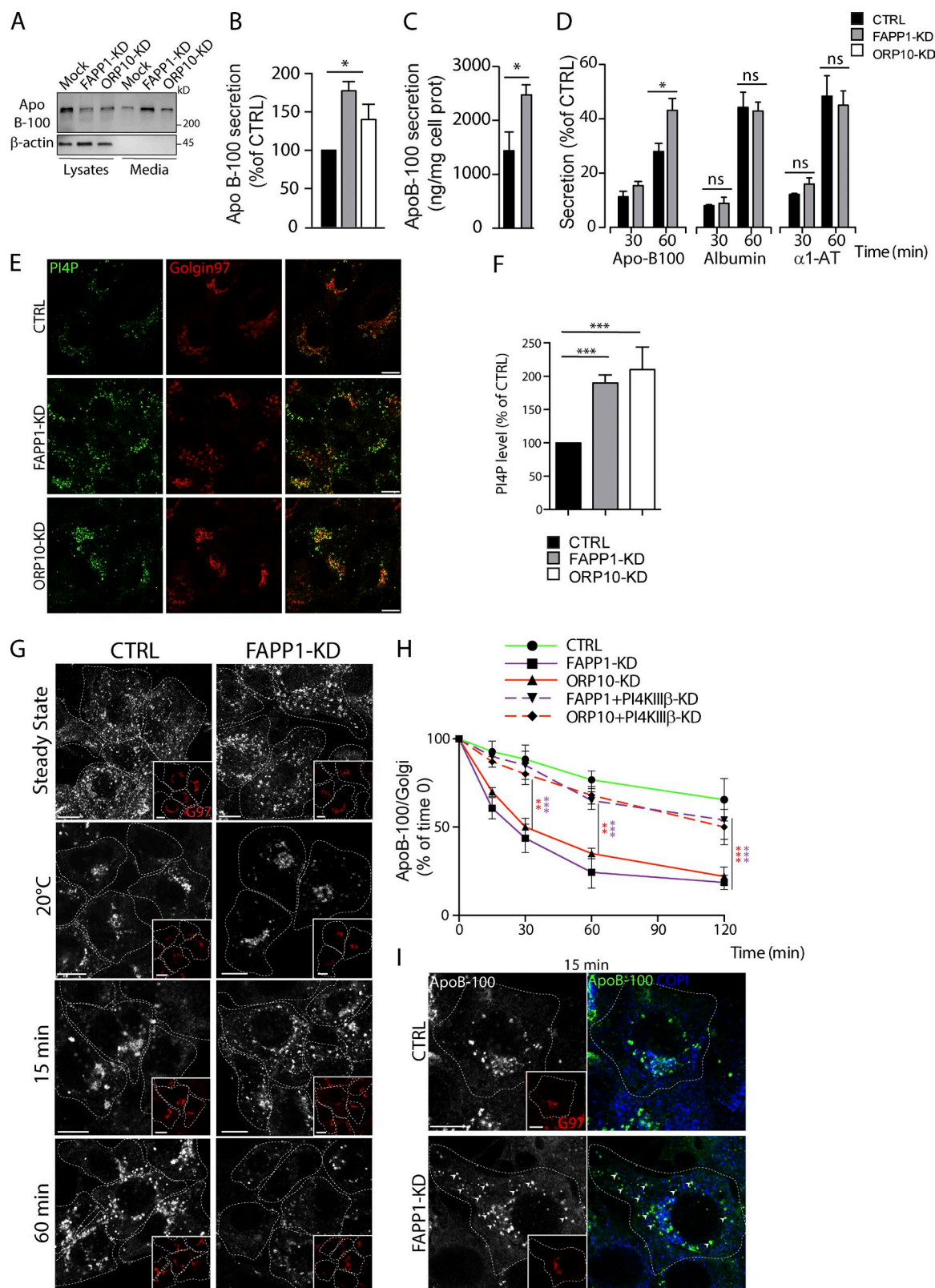


Figure 4. FAPP1 negatively controls ApoB100 export from the TGN in a PI4P-dependent manner. (A) Immunoblot of the medium and cell lysates from Mock, FAPP1-KD, or ORP10-KD cell cultures using the anti-ApoB100 antibody (see Materials and methods). (B) Quantification of the Western blot shown in A. Secretion of ApoB100 (ratio between the amount in the medium and in the cell lysates) expressed as a percentage of control (CTRL). Means \pm SD, $n = 3$. *, $P < 0.05$. (C) ApoB100 secretion evaluated by ELISA from control (CTRL) or FAPP1-KD cells, expressed as the amount (ng) of ApoB100 in the medium normalized for the protein content. *, $P < 0.05$. $n = 3$. (D) ApoB100, albumin, and α 1-anti-trypsin secretion evaluated by pulse-chase. Control or FAPP1-KD cells were incubated as described in Materials and methods. Secretion is expressed as a ratio between the amount of labeled cargo in the medium and the total labeled cargo (medium plus cell lysate). *, $P < 0.05$. $n = 3$. (E) Control, FAPP1-KD, and ORP10-KD HepG2 cells were stained with anti-PI4P (green) and anti-Golgin-97

AAUGGAA-3', #3 5'-GCGAGAGUAUCCUAAAAUUU-3', #4 5'-UCA AAGGGAUAAAGUGGUA-3'; PI4KIII β : #1 5'-UCGGCUGAUAGU GGCAUGAUU-3', #2 5'-UGGCGACAUGUUAACUACUA-3', #3 5'-CGACAUGUUAACUACUAUAA-3'.

HeLa and HepG2 cells were treated for 72 h with Oligofectamine (Life Technologies) or Dharmafect (Dharmacon), respectively, for direct transfection. The knockdown efficiencies of siRNAs used in this study on target protein levels are expressed below as a percentage of residual protein in the knockdown compared with the control (means of three experiments \pm SD).

VAPA: 5.1 ± 2.4 ; VAPB: 4.2 ± 5.1 ; FAPP1: 9.2 ± 4.2 (HeLa cells), and 12.5 ± 5.2 (HepG2 cells); FAPP2: 20 ± 7.5 ; OSBP1: 15.8 ± 5.3 (in OSBP1 KD), 12.9 ± 3.5 (in ORP9 + OSBP1 KD), 18.7 ± 5.9 (in ORP10 + OSBP1 KD), and 16.9 ± 9.1 (in ORP11 + OSBP1 KD); ORP11: 4.5 ± 4.1 (in ORP11 KD), 8.8 ± 6.1 (in ORP9 + ORP11 KD), 11 ± 5.9 (in ORP10 + ORP11 KD), and 10 ± 3.2 (in ORP11 + OSBP1 KD).

ORP10: 12.3 ± 7.5 (in ORP10 KD), 9.9 ± 9.9 (in ORP9 + ORP10 KD), 13.2 ± 5.3 (in ORP10 + ORP11 KD), 10.3 ± 8.1 (in ORP11 + OSBP1 KD), and 15.9 ± 7.3 (HepG2 cells); ORP9: 9.2 ± 4.1 (in ORP9 KD), 7.3 ± 5.7 (in ORP9 + ORP10 KD), 11.2 ± 4.9 (in ORP9 + ORP11 KD), and 5.8 ± 8.7 (in ORP9 + OSBP1 KD).

Immunofluorescence analysis

HeLa or HepG2 cells were grown on coverslips and fixed with 4% PFA for 10 min, washed three times with PBS, blocked, permeabilized for 30 min with blocking solution (0.05% saponin, 0.5% BSA, and 50 mM NH₄Cl in PBS), and incubated with primary antibodies diluted in blocking solution for 1 h at RT. Coverslips were washed with PBS and incubated with fluorochrome-conjugated secondary antibodies (Alexa Fluor 488, Alexa Fluor 568, and Alexa Fluor 633) for 1 h at RT. Fixed cells were mounted in Mowiol and imaged with Plan-Apochromat 63 \times /1.4 oil objective on a Zeiss LSM800 confocal system equipped with an Electronically Switchable Illumination and Detection (ESID) module and controlled by Zen Blue software. For live imaging of the P4M probe (Fig. S1 A), cells were plated in glass-bottomed dishes (MatTek), transfected with the P4M probe for 16 h, and imaged with an LSM800 microscope as described above. During imaging, cells were maintained in complete culture medium in a humidified atmosphere at 37°C. Fluorescence images presented are representative of cells imaged in at least three independent experiments and were processed with FIJI (ImageJ; National Institutes of Health) software. Analysis of PI4P imaging and ER-Golgi contact site quantification is described below and in the corresponding figure legends. Differences between groups were determined using the unpaired Student's *t* test calculated with the GraphPad Prism software. All data are reported as means \pm

SD as indicated in the figure legends. For structured illumination microscopy (SIM; Fig. 2 D), cells were imaged with a Plan-Apochromat 63 \times /1.4 oil objective on a Zeiss LSM880 confocal system. Image stacks of 0.88 μ m thickness were acquired with 0.126 μ m z-steps and 15 images (three angles and five phases per angle) per z-section. The field of view was $\sim 75 \times 75 \mu$ m at 0.065 μ m/pixel, and a SIM grating of 34 μ m was used. Image stacks were processed and reconstructed with Zen software, using the SIM tool in the processing palette.

Rapamycin-induced stabilization of ERTGoCS in cells expressing TGN46-FRB-HA and mCherry-FKBP-Cb5

Rapamycin-induced stabilization of ERTGoCS was performed as described in Venditti et al. (2019). Briefly, to follow the rapamycin-induced stabilization of ERTGoCS, HeLa cells expressing TGN46-FRB-HA-GFP-mCherry-FKBP-Cb5 and treated with the appropriate siRNAs were pretreated with 50 μ g/ml cycloheximide for 30 min, and then treated with 200 nM rapamycin at 37°C at various time points, followed by PFA fixation. Both the cycloheximide and the rapamycin treatments were performed in complete growth medium at 37°C. Cells were then stained with the anti-HA antibody (to verify TGN46 expression) and with a Golgi marker (Golgin-97 to check the overall status of the cells). 15–20 individual fields were imaged (for a total of 150–200 cells) and analyzed to assess mCherry-Cb5 localization. P values were calculated on the basis of mean values from at least three independent experiments.

Immuno-EM

Cells were fixed with mixture of 4% PFA and 0.05% glutaraldehyde in 0.2 M Hepes for 10 min and then with 4% PFA alone for 30 min, followed by incubation with blocking/permeabilizing solution for 30 min. Cells were incubated with the primary anti-GFP rabbit antibody overnight and then with 1.4 nm gold-conjugated Fab' fragment of anti-rabbit IgGs for 2 h. A GoldEnhance EM kit (Nanoprobes) was used to enhance ultrasmall gold particles. The cells were then scraped, pelleted, postfixed in OsO₄ and uranyl acetate, and embedded in Epon.

Generation of FAPP1-KO MEFs

The protocol used to generate FAPP1 KO mice was that described for FAPP2 KO mice in D'Angelo et al. (2013). Briefly, the FAPP1 gene was isolated from a mouse genomic BAC library derived from the 129Sv/J mouse strain (RPCI-22; Children's Hospital Oakland Research Institute, Oakland, CA). An FRT-flanked SA-IRES- β -geo-polyA cassette with an upstream loxP site was inserted into intron 5 and a loxP site was introduced into intron

(red) antibodies. Bar, 10 μ m. (F) Quantification of PI4P levels shown in E. *n* = 3; ***, *P* < 0.001. (G) Golgi-to-PM transport of ApoB100 in control and FAPP1-KD HepG2 cells. Representative images of the distribution of ApoB100 (anti-ApoB100 staining) under steady-state conditions, after a temperature block at 20°C, and after 15 and 60 min of the release from the 20°C temperature block. Insets, Golgin-97 staining. Bar, 10 μ m. (H) Golgi-to-PM transport of ApoB100 in control, FAPP1-KD, ORP10-KD, FAPP1+PI4KIII β -KD, and ORP10+PI4KIII β -KD HepG2 cells. Quantification of Golgi emptying was performed by measuring the ratio between the ApoB100 signal and the Golgin-97 signal at the indicated times after release of the temperature block. Data are means \pm SD expressed as a percentage of the ApoB100 signal in the Golgi compared with the signal at time 0 (i.e., at the end of the temperature block). *n* > 100; three independent experiments. **, *P* < 0.01; ***, *P* < 0.001; Student's *t* test. (I) Control and FAPP1-KD HepG2 cells were treated as described in G, and analyzed after 15 min of the release of the 20°C block. Cells were stained for ApoB100 (gray), Golgin-97 (G97 inset), and COPI (blue). Bar, 10 μ m. The arrowheads indicate ApoB100-positive peripheral structures that are probably post-Golgi carriers since they lack a COPI coat.

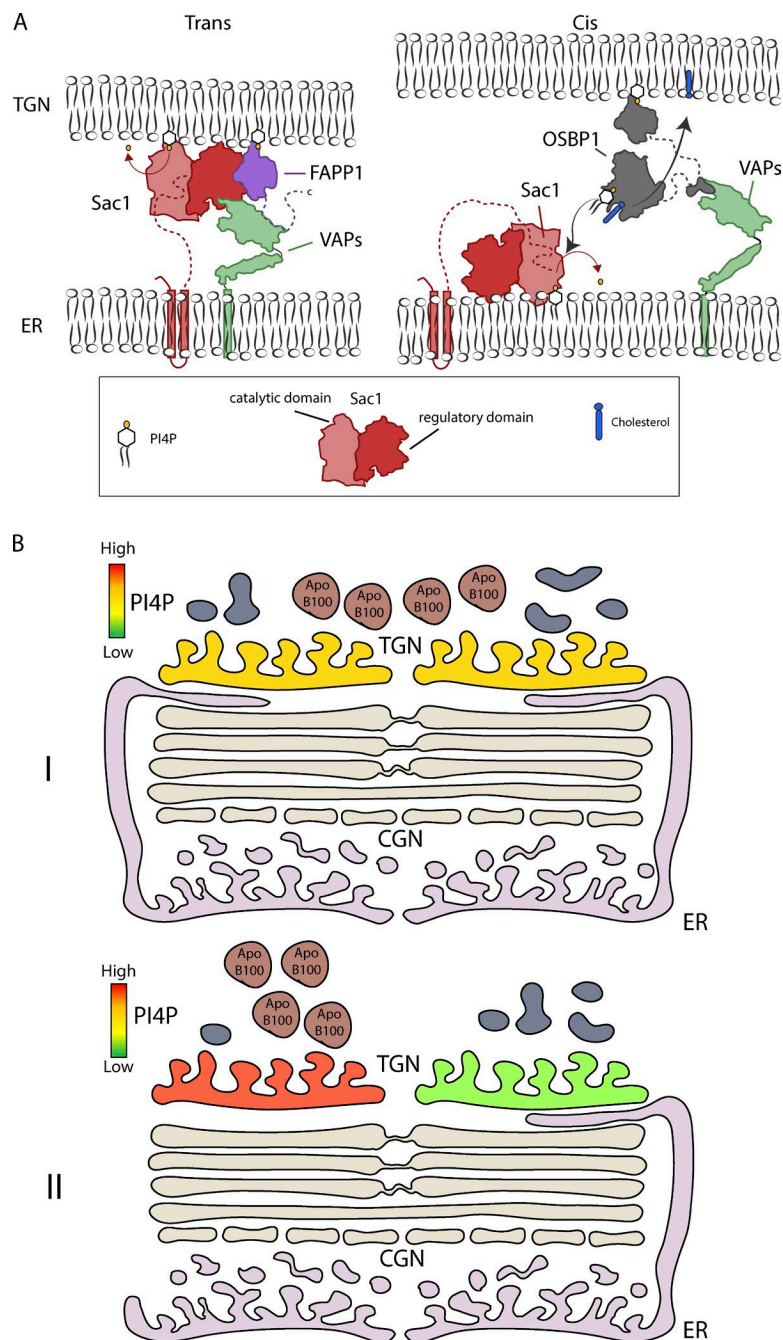


Figure 5. Models of the distribution of modes of action of Sac1 and of the distribution of ERTGoCS and PI4P among Golgi stacks. (A) Two possible modes of action of Sac1 at the ERTGoCS. The width of ERTGoCS ranges from 5 to 20 nm (Venditti et al., 2019). We envisage that the in-trans activity of Sac1 may occur only at the tighter contact sites and only when FAPP1 is present. In the cis mode, Sac1 acts on PI4P that is transferred from the TGN to the ER by OSBP1 in exchange for cholesterol. In this mode, Sac1 can also operate at contact sites that have a greater distance between the opposing membranes since OSBP1 can in principle shuttle between the TGN and the ER. **(B)** Two possible scenarios of ERTGoCS and PI4P distribution among Golgi stacks. I: The TGN of every Golgi stack can engage in ERTGoCS at any given time. PI4P levels are kept equal and at a medium level in the TGN of all the stacks. ApoB100 export also occurs from the TGN of every stack but at a low rate. II: Only TGN from a subset of Golgi stacks can engage in ERTGoCS. PI4P levels are heterogeneous in the TGN of different stacks, some with high levels of PI4P (devoid of ERTGoCS) and others with low PI4P levels. ApoB100 export occurs exclusively and at a high rate from a TGN with high PI4P levels.

7 in the FAPP1 targeting vector. This construct was used for the generation of the heterozygous FAPP1 *geo/+* mice. Homozygous FAPP1 *geo/geo* mice (FAPP1 KO mice) were obtained by mating. The absence of FAPP1 was verified by Western blot and by PCR analysis. The PCR primers used were 5'-AAAACACCCAGTGGT CAGGCTAGCA-3' (Primer 1), 5'-ATAACTGAGCACCAGGAGGAG AAGG-3' (Primer 2), and 5'-CCGTACAGTTCACAAAGGCATCCT-3' (Primer 3), where primer pair 1 and 2 detected the WT allele and primers 1 and 3 detected the *geo* allele of FAPP1.

All animal procedures were performed in accordance with the guidelines of the Animal Care and Experimentation Committee of Gunma University, and all animals were bred in the Institute of Animal Experience Research of Gunma University.

MEFs were isolated from E13.5 embryos. Three embryos were pooled to generate each single MEF clone. Briefly, after isolation and removal of internal organs, the embryos were trypsinized (0.125% trypsin-EDTA) at 37°C for 15 min and put in culture in DMEM with 20% FCS plus amphotericin and penicillin/streptomycin for the first week and kept for several passages.

PI4P detection

PI4P was detected by four independent approaches: three based on the imaging of PI4P in living or fixed cells and one on a biochemical PI4P mass assay on isolated Golgi fractions using recombinant PIP5K1C.

PI4P imaging

PI4P was detected using three independent imaging approaches: staining of PI4P with a monoclonal anti-PI4P antibody (Echelon) following the protocol described by Hammond et al. (2009), detection of PI4P using two different genetically encoded probes (P4M and P4C, corresponding to the PI4P-binding domains of the two *Legionella pneumophila* effectors SidM and SidC, respectively; Hammond et al., 2014; Luo et al., 2015), and staining of PI4P in streptolysin O (SLO)-permeabilized cells with a recombinant PI4P probe produced in *Escherichia coli* (GST-FAPP PH domain) as previously described (Godi et al., 2004).

Quantification of Golgi PI4P stained with the anti-PI4P antibody

Hela cells were double stained for PI4P and for the TGN with anti-PI4P and anti-Golgin-97 antibodies, respectively, following the protocol of Hammond et al. (2009). Briefly, cells were fixed with 2% PFA for 15 min at RT, washed three times in PBS supplemented with 50 mM NH₄Cl, and permeabilized for 5 min by the addition of 20 μM digitonin in Buffer A (20 mM Pipes, pH 6.8, 137 mM NaCl, and 2.7 mM KCl) for 5 min. After three rinses in Buffer A, cells were blocked for 45 min with blocking solution (Buffer A supplemented with 5% [vol/vol] FBS and 50 mM NH₄Cl) and incubated with primary antibodies diluted in blocking solution for 1 h. Cells were then washed with Buffer A, incubated with fluorescence-conjugated secondary antibodies for 1 h, and finally postfixed for 5 min in 2% PFA. 10–15 fields (each containing 10–15 cells) were randomly sampled and imaged at the same microscope settings (i.e., laser power and detector amplification) and below pixel saturation. The mean intensity per cell was determined using the ImageJ software. For PI4P level assessment, a mask using the TGN marker Golgin-97 was generated for each cell, and the mean intensities of both PI4P and Golgin-97 were measured in those regions. After background subtraction, the PI4P values were normalized singularly using their own Golgin-97 values.

Quantification of Golgi PI4P detected with P4C

Both P4M and P4C, expressed for 16 h in HeLa cells, exhibited a clear Golgi localization in living cells, but only P4C preserved a strong association with the Golgi complex after fixation, consistent with its higher affinity for PI4P as compared with P4M (Luo et al., 2015). Quantification of Golgi PI4P detected with P4C was performed both in live cells by fluorescence loss in photobleaching (FLIP) and in fixed cells. FLIP was performed in cells expressing GFP-P4C by bleaching iteratively (100 times) the GFP-associated fluorescence in the entire cell area except for the Golgi area and monitoring the Golgi-associated fluorescence over time. The relative fluorescence intensity, expressed as a percentage of prebleaching fluorescence, was plotted. Reflecting the increase in Golgi PI4P, the depletion of VAPs and FAPP1 induced a slowdown of the FLIP-induced decay curves of P4C from the Golgi area. For quantification of P4C associated with the Golgi complex in fixed cells, HeLa cells expressing GFP-P4C were stained for a TGN marker (Golgin-97) used to generate a mask in the Golgi region. The mean intensity of GFP-P4C was measured in the Golgi region and normalized for the mean intensity of an equivalent area outside the Golgi region. Golgi PI4P was expressed as the

ratio between GFP-P4C fluorescence intensity in the Golgi region and in the equivalent extra-Golgi area.

Quantification of the GST-FAPP PH domain on the Golgi complex was performed as described (Godi et al., 2004): cells were incubated with 1 U/ml SLO in SLO buffer (20 mM Hepes, pH 7.2, 110 mM Mg(OAc)₂, and 1 mM DTT) for 10 min at 4°C. Cells were then washed twice and incubated in permeabilization buffer (25 mM Hepes, pH 6.95, 125 mM KOAc, 2.5 mM Mg(OAc)₂, 10 mM glucose, 1 mM DTT, 1 mM ATP, 5 mM creatine phosphate, 7.3 U/ml creatine phosphokinase, and 1 mg/ml rat liver cytosol) for 5 min at 37°C and then in permeabilization buffer containing 1 μM of GST or GST-FAPP-PH for an additional 5 min. Cells were then fixed with 4% PFA and processed for immunofluorescence microscopy, as described above. Quantification was performed as described above for the PI4P antibody, with the exception that the Golgi marker used was Giantin instead of Golgin-97.

PI4P mass assay with recombinant PIP5K1C

Golgi fractions, identified as fractions enriched for Golgi markers and devoid of PM markers, were isolated as described (Balch et al., 1984). Golgi fractions (60 μg) were washed with 0.2 M KCl in 20 mM Hepes, pH 7.4, and 10 mM MgCl₂ and centrifuged at 14,000 rpm for 20 min. Pellets were resuspended in 20 mM Hepes and incubated for 30 min at 32°C in reaction buffer (20 mM Hepes, pH 7.4, 10 mM MgCl₂, 40 μM ATP, and 200 μM sodium orthovanadate) with 2 μCi [γ-³²P]-ATP, in the presence or absence of 30 ng of recombinant PIP5K1C in a final reaction volume of 100 μl. The reaction was stopped by adding 20 μl 8 M HCl, and lipids were extracted with chloroform:methanol (1:1). The organic phase was dried and spotted on silica-gel TLC plates (Millipore), resolved with a mixture of chloroform:methanol:ammonium hydroxide: water (60:47:2:11 vol/vol/vol/vol), and analyzed by TLC. A sample where PIP5K1C was incubated with 3 μM porcine brain PI4P in reaction buffer with 2 μCi [γ-³²P]-ATP was taken as a reference for PI4,5P₂. The radioactive products were detected with a Typhoon TLA 9500.

BioID2 experiments and immunoprecipitation

HeLa cells were transfected with the Sac1-BioID2 or FAPP1-BioID2 constructs. 16 h post-transfection, cells were incubated with 50 μM biotin for an additional 24 h before lysis and processed as described by Roux et al. (2013).

Cell extracts from untransfected HeLa cells or cells expressing GFP-FAPP1 or GFP-Sac1 were immune-precipitated using anti-GFP antibody, and the immune-precipitates were analyzed by Western blot or by liquid chromatography-tandem mass spectrometry (Central Proteomics Facility, Sir William Dunn Pathology School, Oxford University, Oxford, UK). Control immune precipitates were obtained with anti-GFP antibody in cells expressing soluble GFP.

Recombinant proteins and pull-down (PD) experiments

All recombinant proteins were expressed in BL21 DE3 or Rosetta DE3 *E. coli* (Merck). GST-tagged proteins (FAPP1-FL, FAPP1 residues 1–100, FAPP1 residues 97–300, VAPA, VAPB, and GST alone) expressed from the pGEX plasmid were purified using Glutathione Sepharose 4B (GE Healthcare). His-tagged proteins expressed

from pTrcHis2 (Sac1 residues 1–522 and Sac1 residues 1–188), and the His-SUMO-tagged proteins (FAPP1, VAPA, and VAPB), were purified using Ni-NTA agarose (Qiagen), according to the manufacturer's instructions. The PD experiments were performed as previously described (Venditti et al., 2012). Briefly, 0.2 μ M His-tagged proteins (Sac1 FL, 1–522 and 1–188 forms, and VAPA; Fig. 2) were incubated with GST-fusion proteins (FAPP1 FL, 1–100, or 97–300 forms, VAPA and VAPB) and GST alone (0.2 μ M). After overnight incubation at 4°C in 300 μ l binding buffer (50 mM Tris, pH 7.4, 100 mM NaCl, 1 mg/ml BSA, 0.1% Triton X-100, and 0.1% NP-40), glutathione-beads were added, incubated for 2 h at 4°C, washed five times (50 mM Tris, pH 7.4, and 100 mM NaCl), eluted, and analyzed by SDS-PAGE.

Liposome preparation, Sac1 phosphatase, and PI4P extraction assays

PI4P-containing liposomes were prepared starting from lipid stock solutions in chloroform using the following molar ratios of lipids: DOPC, 45%; DOPE, 20%; DOPS, 5%; and porcine brain PI4P, 30%. Lipid mixtures in chloroform were dried under a nitrogen stream in a glass tube and hydrated in 50 mM Hepes, pH 7.4, 120 mM KAc, and 1 mM $MgCl_2$ to produce a 2-mM lipid suspension. Lipid suspensions were transferred to LoBind tubes (Eppendorf), subjected to six freeze-thaw cycles (frozen in liquid nitrogen and thawed at 37°C), and extruded using a polycarbonate membrane with a pore diameter of 100 nm.

To measure the in-cis activity of Sac1, 2 mol% DOGS-Ni-NTA was used in the preparation of the PI4P-containing liposomes at the expense of DOPC. The DOGS-Ni-NTA-containing liposomes were preincubated for 30 min at RT with 6xHis-hSac1^{1–522} (0.5 μ M) to allow binding of the protein to the lipids. 20 μ l of the liposomes was transferred to a well of a 384-well plate and brought to 100 μ l with the addition of reaction buffer (50 mM Hepes, pH 7.4, 120 mM KAc, and 1 mM $MgCl_2$). Since hSac1 needs to be in a reduced conformation to be enzymatically active in vitro, 1 mM DTT was added to start the reactions that were performed at 32°C. Aliquots (12.5 μ l) of the mixture were withdrawn at different time points and added to 10 μ l of 200 mM N-Ethylmaleimide to stop the reaction. Sac1 phosphatase activity was measured based on the amount of phosphate released in solution by adding 50 μ l of malachite green reagent and reading the absorbance at 620 nm after 20 min.

To measure the in-trans activity of Sac1, 6xHis-hSac1^{1–522} (0.5 μ M) was preincubated for 30 min at RT with 2 mM DOPC liposomes containing 2 mol% DOGS-Ni-NTA. 20 μ l of these liposomes were mixed with 20 μ l of PI4P-containing liposomes and 60 μ l of DTT-containing reaction buffer and assayed as above. In agreement with previous reports (Mesmin et al., 2013), the spontaneous in-trans activity of Sac1 is low (Fig. 2 F), and the lag phase observed under these conditions is likely due to the fact that Sac1 is allosterically stimulated by its product, PtdIns (Zhong et al., 2012). This explains why the reaction is slower, showing a lag, at the very beginning of the in-trans reaction, i.e., when the product concentration is particularly low. To measure the effects of FAPP1, either GST or GST-FAPP1 was added to the reaction mixture at the indicated final concentrations.

To measure Sac1 activity on soluble PI4P, 1 μ M 6xHis-hSac1^{1–522} was incubated for 30 min at RT with 2 mM DOPC liposomes

containing 2 mol% DOGS-Ni-NTA. 40 μ l of these liposomes were mixed with 100 μ M diC8-PI4P in reaction buffer.

PI4P extraction from membranes was measured using liposomes having the following molar ratio of lipids: DOPC, 68%; DOPE, 19%; DOPS, 5%; 2% TopFLUOR-PI4P; and 6% DiIC18, which quenches TopFLUOR-PI4P fluorescence when present on the same vesicle. TopFLUOR-PI4P release from vesicles results in an increase in the fluorescence emission (Ex485/Em520).

Liposome tethering assay

The liposome tethering assay was performed as described in Saheki et al. (2016). Briefly, 6xHis-hSac1^{1–522} (1 μ M) was preincubated for 30 min at RT with 2 mM DOPC liposomes containing 2 mol% DOGS-Ni-NTA. 10 μ l of these liposomes were mixed with 10 μ l of PI4P-containing liposomes and 30 μ l reaction buffer containing either FAPP1 (at the indicated concentrations) or a His-tagged version of the PH domain of FAPP1 (6xHis-GST-FAPP1 PH domain) that binds both DOGS-Ni-NTA liposomes containing Sac1 (via its His tag) and the PI4P-containing liposomes (via the PH domain of FAPP1), thus acting as a tether between the two liposome populations. Liposome aggregation was assessed by measuring the absorbance at 405 nm every 15 s over 15 min at 32°C using a Neo2 Microplate Reader (Biotech). The absorbance before protein addition was set to 0.

Optogenetics

The optogenetics control system to visualize ERTGoCS is based on light-induced dimerization of the iLID (Lungu et al., 2012; Guntas et al., 2015) adapted version described in the plasmid construction section.

HeLa cells cotransfected with the opto-ERTGoCS and iRFP-P4M constructs were analyzed using time-lapse microscopy. The mCherry-LOV-SsrA-Cb5 conformational change was induced using one blue light-enhanced pulse (100% power 488 nm laser) followed by acquisition of the three channels. This procedure was repeated each frame during the illumination step only (~10 min).

Before and after illumination, images were acquired using the mCherry channel in order to analyze mCherry-LOV-SsrA-Cb5 localization, and the GFP channel was only acquired during illumination to analyze TGN-GFP-SspB. The reversibility was performed by image acquisition for the same period of time, removing the 488-nm pulses. PI4P levels were measured throughout the entire acquisition using the iRFP670 channel. The time-lapse images from the three channels were combined in series using ImageJ and the region of interest defined by the GFP signal after illumination. The fluorescence intensity of each mCherry-Cb5 and iRFP-P4M frame was measured using the region of interest and plotted after background subtraction as a percentage of the starting point.

For selected experiments, HeLa cells were transfected with the opto-ERTGoCS, subjected to activation with blue light, fixed, and stained for a TGN marker (Golgin-97) and PI4P.

ApoB100 secretion

HepG2 cells were incubated for the indicated times in MEM containing 5% delipidated serum. ApoB100 in cell lysates and in the medium was determined using both Western blot with a specific

antibody (Rockland Immunochemicals) and a sandwich ELISA (Mabtech), as described in Nissilä et al. (2012).

For pulse-chase experiments, HepG2 cells were grown in 10% FBS/MEM. After mock or siRNA treatment, cells were washed with warm PBS and incubated in pulse medium (methionine/cysteine-free DMEM) supplemented with 2 mM L-glutamine (Sigma-Aldrich) and 100 $\mu\text{Ci ml}^{-1}$ [^{35}S]-methionine/cysteine (NEG77200; EasyTag Express Protein Labeling Mix; Perkin-Elmer) for 30 min for ApoB100 and 5 min for albumin and α 1-anti-trypsin, as previously described (Nissilä et al., 2012; Venditti et al., 2012). The media and cell lysates were immunoprecipitated using specific antibodies, analyzed by Western blot, and quantified with Typhoon TLA 9500. The ratio between the labeled cargo (ApoB100, albumin, and α 1-anti-trypsin) in the supernatant and the total amount (supernatant plus cell lysate) was taken as measure of secretion at the indicated times.

ApoB100 trafficking out of the Golgi complex was imaged, adopting a synchronization protocol. HepG2 cells were seeded onto coverslips for 72 h and then incubated at 20°C for 8 h in MEM supplemented with 5% delipidated serum to favor the accumulation of ApoB100 in the TGN. To allow TGN exit of ApoB100, the temperature was shifted to 37°C for the indicated times (in the same medium with addition of 50 $\mu\text{g ml}^{-1}$ cycloheximide). At various times, cells were fixed (4% PFA, 10 min, RT) and stained for ApoB100 and for TGN (using the anti-ApoB100 and anti-Golgin 97 antibodies).

The amount of ApoB-100 in the Golgi was calculated by measuring the ApoB100 signal in Golgin-97-positive structures. The value measured at time 0 at the end of the 20°C block was taken as 100%. At least 100 cells for each time point were acquired below saturation level and analyzed, using ImageJ software.

Online supplemental material

Fig. S1 shows how the depletion of VAPs, ORP10, or FAPP1 increases Golgi PI4P. Fig. S2 shows that FAPP1 interacts with VAP and with Sac1 and stimulates the in-trans phosphatase activity of Sac1. Table S1 shows a list of primers and cloning strategies used in this study. Video 1 shows the reversible light-induced stabilization of ERTGoCS and the decrease of TGN PI4P via optogenetics.

Acknowledgments

We thank all the colleagues who provided the reagents listed in Materials and methods and Andrea Ballabio, Carmine Settembre, Luis Galletta, Graciana Diez Roux, Francesca Zappa, Leopoldo Staiano, and Cathal Wilson for helpful discussion.

M.A. De Matteis acknowledges the support of Telethon (grant TGM11CB1), the Italian Association for Cancer Research (grant IG2013_14761), and European Research Council Advanced Investigator grant 670881 (SYSMET). R. Venditti acknowledges the University of Naples Federico II (grant STAR2017 Linea1). V.M. Olkkonen acknowledges the support of the Academy of Finland (grant 285223) and the Sigrid Juselius Foundation. D.L. Medina acknowledges the support of grants from the ML4 foundation, the Cure SanFilippo Foundation, and EU Horizon2020 grant 666918 (BATCure).

The authors declare no competing financial interests.

Author contributions: R. Venditti, L.R. Rega, and M.A. De Matteis conceived the work. R. Venditti, L.R. Rega, and M.C. Masone planned and analyzed most of the experiments. E. Polishchuk performed EM analyses. I.C. Serrano and M. Santoro developed the optogenetics approach. G. Di Tullio performed the protein-protein interaction studies and the PIP5K1C assay. V.M. Olkkonen provided ORP10 reagents and discussed the ORP10 relevant data. A. Harada developed the FAPP1 KO mice, D.L. Medina performed the analysis of the rapamycin-induced stabilization of ERTGoCS. R. La Montagna and G. Di Tullio performed the in vitro Sac1 activity studies. M.A. De Matteis conceptualized the work and strategy and wrote the manuscript, together with R. Venditti and M.C. Masone.

Submitted: 5 December 2018

Revised: 14 December 2018

Accepted: 19 December 2018

References

- Bajaj Pahuja, K., J. Wang, A. Blagoveshchenskaya, L. Lim, M.S. Madhusudan, P. Mayinger, and R. Schekman. 2015. Phosphoregulatory protein 14-3-3 facilitates SAC1 transport from the endoplasmic reticulum. *Proc. Natl. Acad. Sci. USA*. 112:E3199–E3206. <https://doi.org/10.1073/pnas.1509119112>
- Balch, W.E., W.G. Dunphy, W.A. Braell, and J.E. Rothman. 1984. Reconstitution of the transport of protein between successive compartments of the Golgi measured by the coupled incorporation of N-acetylglucosamine. *Cell*. 39:405–416. [https://doi.org/10.1016/0092-8674\(84\)90019-9](https://doi.org/10.1016/0092-8674(84)90019-9)
- Balla, T. 2013. Phosphoinositides: tiny lipids with giant impact on cell regulation. *Physiol. Rev.* 93:1019–1137. <https://doi.org/10.1152/physrev.00028.2012>
- Caldieri, G., E. Barbieri, G. Nappo, A. Raimondi, M. Bonora, A. Conte, L.G.G.C. Verhoef, S. Confalonieri, M.G. Malabarba, F. Bianchi, et al. 2017. Reticulon 3-dependent ER-PM contact sites control EGFR nonclathrin endocytosis. *Science*. 356:617–624. <https://doi.org/10.1126/science.aah6152>
- Cheong, F.Y., V. Sharma, A. Blagoveshchenskaya, V.M.J. Oorschot, B. Brankatschk, J. Klumperman, H.H. Freeze, and P. Mayinger. 2010. Spatial regulation of Golgi phosphatidylinositol-4-phosphate is required for enzyme localization and glycosylation fidelity. *Traffic*. 11:1180–1190. <https://doi.org/10.1111/j.1600-0854.2010.01092.x>
- Chung, J., F. Torta, K. Masai, L. Lucast, H. Czaplá, L.B. Tanner, P. Narayanaswamy, M.R. Wenk, F. Nakatsu, and P. De Camilli. 2015. INTRACELLULAR TRANSPORT. PI4P/phosphatidylserine countertransport at ORP5- and ORP8-mediated ER-plasma membrane contacts. *Science*. 349:428–432. <https://doi.org/10.1126/science.aab1370>
- D'Angelo, G., E. Polishchuk, G. Di Tullio, M. Santoro, A. Di Campli, A. Godi, G. West, J. Bielawski, C.-C. Chuang, A.C. van der Spoel, et al. 2007. Glycosphingolipid synthesis requires FAPP2 transfer of glucosylceramide. *Nature*. 449:62–67. <https://doi.org/10.1038/nature06097>
- D'Angelo, G., M. Vicinanza, A. Di Campli, and M.A. De Matteis. 2008. The multiple roles of PtdIns(4)P -- not just the precursor of PtdIns(4,5)P2. *J. Cell Sci.* 121:1955–1963. <https://doi.org/10.1242/jcs.023630>
- D'Angelo, G., T. Uemura, C.C. Chuang, E. Polishchuk, M. Santoro, H. Ohvo-Rekilä, T. Sato, G. Di Tullio, A. Varriale, S. D'Auria, et al. 2013. Vesicular and non-vesicular transport feed distinct glycosylation pathways in the Golgi. *Nature*. 501:116–120. <https://doi.org/10.1038/nature12423>
- De Matteis, M.A., A. Di Campli, and G. D'Angelo. 2007. Lipid-transfer proteins in membrane trafficking at the Golgi complex. *Biochim. Biophys. Acta*. 1771:761–768. <https://doi.org/10.1016/j.bbalip.2007.04.004>
- De Matteis, M.A., C. Wilson, and G. D'Angelo. 2013. Phosphatidylinositol-4-phosphate: the Golgi and beyond. *BioEssays*. 35:612–622. <https://doi.org/10.1002/bies.201200180>
- Dickson, E.J., J.B. Jensen, O. Vivas, M. Kruse, A.E. Traynor-Kaplan, and B. Hille. 2016. Dynamic formation of ER-PM junctions presents a lipid phosphatase to regulate phosphoinositides. *J. Cell Biol.* 213:33–48. <https://doi.org/10.1083/jcb.201508106>
- Dong, R., Y. Saheki, S. Swarup, L. Lucast, J.W. Harper, and P. De Camilli. 2016. Endosome-ER Contacts Control Actin Nucleation and Retromer

- Function through VAP-Dependent Regulation of PI4P. *Cell*. 166:408–423. <https://doi.org/10.1016/j.cell.2016.06.037>
- Dowler, S., R.A. Currie, D.G. Campbell, M. Deak, G. Kular, C.P. Downes, and D.R. Alessi. 2000. Identification of pleckstrin-homology-domain-containing proteins with novel phosphoinositide-binding specificities. *Biochem. J.* 351:19–31. <https://doi.org/10.1042/bj3510019>
- Godi, A., A. Di Campli, A. Konstantakopoulos, G. Di Tullio, D.R. Alessi, G.S. Kular, T. Daniele, P. Marra, J.M. Lucocq, and M.A. De Matteis. 2004. FAPPs control Golgi-to-cell-surface membrane traffic by binding to ARF and PtdIns(4)P. *Nat. Cell Biol.* 6:393–404. <https://doi.org/10.1038/ncb1119>
- Grecco, H.E., and P.I.H. Bastiaens. 2013. Quantifying cellular dynamics by fluorescence resonance energy transfer (FRET) microscopy. *Curr. Protoc. Neurosci.* Chapter 5:Unit 5.22.
- Guntas, G., R.A. Hallett, S.P. Zimmerman, T. Williams, H. Yumerefendi, J.E. Bear, and B. Kuhlman. 2015. Engineering an improved light-induced dimer (iLID) for controlling the localization and activity of signaling proteins. *Proc. Natl. Acad. Sci. USA*. 112:112–117. <https://doi.org/10.1073/pnas.1417910112>
- Hammond, G.R.V., G. Schiavo, and R.F. Irvine. 2009. Immunocytochemical techniques reveal multiple, distinct cellular pools of PtdIns4P and PtdIns(4,5)P₂. *Biochem. J.* 422:23–35. <https://doi.org/10.1042/BJ20090428>
- Hammond, G.R.V., M.P. Machner, and T. Balla. 2014. A novel probe for phosphatidylinositol 4-phosphate reveals multiple pools beyond the Golgi. *J. Cell Biol.* 205:113–126. <https://doi.org/10.1083/jcb.201312072>
- Hanada, K., K. Kumagai, S. Yasuda, Y. Miura, M. Kawano, M. Fukasawa, and M. Nishijima. 2003. Molecular machinery for non-vesicular trafficking of ceramide. *Nature*. 426:803–809. <https://doi.org/10.1038/nature02188>
- Hossain, T., A. Riad, S. Siddiqi, S. Parthasarathy, and S.A. Siddiqi. 2014. Mature VLDL triggers the biogenesis of a distinct vesicle from the trans-Golgi network for its export to the plasma membrane. *Biochem. J.* 459:47–58. <https://doi.org/10.1042/BJ20131215>
- Hsu, F., and Y. Mao. 2015. The structure of phosphoinositide phosphatases: Insights into substrate specificity and catalysis. *Biochim. Biophys. Acta*. 1851:698–710. <https://doi.org/10.1016/j.bbali.2014.09.015>
- Koriyama, H., H. Nakagami, T. Katsuya, H. Akasaka, S. Saitoh, K. Shimamoto, T. Ogihara, Y. Kaneda, R. Morishita, and H. Rakugi. 2010. Variation in OSBPL10 is associated with dyslipidemia. *Hypertens. Res.* 33:511–514. <https://doi.org/10.1038/hr.2010.28>
- Levine, T.P., and S. Munro. 2002. Targeting of Golgi-specific pleckstrin homology domains involves both PtdIns 4-kinase-dependent and -independent components. *Curr. Biol.* 12:695–704. [https://doi.org/10.1016/S0960-9822\(02\)00779-0](https://doi.org/10.1016/S0960-9822(02)00779-0)
- Lungu, O.I., R.A. Hallett, E.J. Choi, M.J. Aiken, K.M. Hahn, and B. Kuhlman. 2012. Designing photoswitchable peptides using the AsLOV2 domain. *Chem. Biol.* 19:507–517. <https://doi.org/10.1016/j.chembiol.2012.02.006>
- Luo, X., D.J. Wasilko, Y. Liu, J. Sun, X. Wu, Z.-Q. Luo, and Y. Mao. 2015. Structure of the Legionella Virulence Factor, SidC Reveals a Unique PI(4)P-Specific Binding Domain Essential for Its Targeting to the Bacterial Phagosome. *PLoS Pathog.* 11:e1004965. <https://doi.org/10.1371/journal.ppat.1004965>
- Mesmin, B., J. Bigay, J. Moser von Filseck, S. Lacas-Gervais, G. Drin, and B. Antonny. 2013. A four-step cycle driven by PI(4)P hydrolysis directs sterol/PI(4)P exchange by the ER-Golgi tether OSBP. *Cell*. 155:830–843. <https://doi.org/10.1016/j.cell.2013.09.056>
- Murphy, S.E., and T.P. Levine. 2016. VAP, a Versatile Access Point for the Endoplasmic Reticulum: Review and analysis of FFAT-like motifs in the VAPome. *Biochim. Biophys. Acta*. 1861(8 Pt B):952–961. <https://doi.org/10.1016/j.bbali.2016.02.009>
- Ngo, M., and N.D. Ridgway. 2009. Oxysterol binding protein-related Protein 9 (ORP9) is a cholesterol transfer protein that regulates Golgi structure and function. *Mol. Biol. Cell*. 20:1388–1399. <https://doi.org/10.1091/mbc.e08-09-0905>
- Nissilä, E., Y. Ohsaki, M. Weber-Boyvat, J. Perttälä, E. Ikonen, and V.M. Olkkonen. 2012. ORP10, a cholesterol binding protein associated with microtubules, regulates apolipoprotein B-100 secretion. *Biochim. Biophys. Acta*. 1821:1472–1484. <https://doi.org/10.1016/j.bbali.2012.08.004>
- Perttälä, J., K. Merikanto, J. Naukkarinen, I. Surakka, N.W. Martin, K. Tanshuanpää, V. Grimard, M.-R. Taskinen, C. Thiele, V. Salomaa, et al. 2009. OSBPL10, a novel candidate gene for high triglyceride trait in dyslipidemic Finnish subjects, regulates cellular lipid metabolism. *J. Mol. Med. (Berl.)*. 87:825–835. <https://doi.org/10.1007/s00109-009-0490-z>
- Phillips, M.J., and G.K. Voeltz. 2016. Structure and function of ER membrane contact sites with other organelles. *Nat. Rev. Mol. Cell Biol.* 17:69–82. <https://doi.org/10.1038/nrm.2015.8>
- Rohde, H.M., F.Y. Cheong, G. Konrad, K. Pahi, P. Mayinger, and G. Boehmelt. 2003. The human phosphatidylinositol phosphatase SAC1 interacts with the coatomer I complex. *J. Biol. Chem.* 278:52689–52699. <https://doi.org/10.1074/jbc.M307983200>
- Roux, K.J., D.I. Kim, and B. Burke. 2013. BioID: A screen for protein-protein interactions. Vol. 74. Current Protocols in Protein Science., Unit 19.23. John Wiley & Sons, Inc., Hoboken, NJ.
- Saheki, Y., X. Bian, C.M. Schauder, Y. Sawaki, M.A. Surma, C. Klose, F. Pinet, K.M. Reinisch, and P. De Camilli. 2016. Control of plasma membrane lipid homeostasis by the extended synaptotagmins. *Nat. Cell Biol.* 18:504–515. <https://doi.org/10.1038/ncb3339>
- Sohn, M., M. Korzeniowski, J.P. Zewe, R.C. Wills, G.R.V. Hammond, J. Humpolickova, L. Vrzal, D. Chalupska, V. Veverka, G.D. Fairn, et al. 2018. PI(4,5)P₂ controls plasma membrane PI4P and PS levels via ORP5/8 recruitment to ER-PM contact sites. *J. Cell Biol.* 217:1797–1813. <https://doi.org/10.1083/jcb.201710095>
- Stefan, C.J., A.G. Manford, D. Baird, J. Yamada-Hanff, Y. Mao, and S.D. Emr. 2011. Osh proteins regulate phosphoinositide metabolism at ER-plasma membrane contact sites. *Cell*. 144:389–401. <https://doi.org/10.1016/j.cell.2010.12.034>
- Valente, C., G. Turacchio, S. Mariggiò, A. Pagliuso, R. Gaibisso, G. Di Tullio, M. Santoro, F. Formigini, S. Spanò, D. Piccini, et al. 2012. A 14-3-3γ dimer-based scaffold bridges CtBP1-S/BARS to PI(4)KIIIβ to regulate post-Golgi carrier formation. *Nat. Cell Biol.* 14:343–354. <https://doi.org/10.1038/ncb2445>
- Venditti, R., T. Scanu, M. Santoro, G. Di Tullio, A. Spaar, R. Gaibisso, G.V. Beznoussenko, A.A. Mironov, A. Mironov, L. Zelante, et al. 2012. Sedlin controls the ER export of procollagen by regulating the Sar1 cycle. *Science*. 337:1668–1672. <https://doi.org/10.1126/science.1224947>
- Venditti, R., L.R. Rega, M.C. Masone, M. Santoro, E. Polishchuk, D. Sarnataro, S. Paladino, S. D'Auria, A. Varriale, V.M. Olkkonen, et al. 2019. Molecular determinants of ER-Golgi contacts identified through a new FRET-FLIM system. *J. Cell Biol.* <https://doi.org/10.1083/jcb.201812020>
- Wood, C.S., C.-S. Hung, Y.-S. Huoh, C.J. Mousley, C.J. Stefan, V. Bankaitis, K.M. Ferguson, and C.G. Burd. 2012. Local control of phosphatidylinositol 4-phosphate signaling in the Golgi apparatus by Vps74 and Sac1 phosphoinositide phosphatase. *Mol. Biol. Cell*. 23:2527–2536. <https://doi.org/10.1091/mbc.e12-01-0077>
- Zewe, J.P., R.C. Wills, S. Sangappa, B.D. Goulden, and G.R. Hammond. 2018. SAC1 degrades its lipid substrate PtdIns4P in the endoplasmic reticulum to maintain a steep chemical gradient with donor membranes. *eLife*. 7:e35588. <https://doi.org/10.7554/eLife.35588>
- Zhong, S., F. Hsu, C.J. Stefan, X. Wu, A. Patel, M.S. Cosgrove, and Y. Mao. 2012. Allosteric activation of the phosphoinositide phosphatase Sac1 by anionic phospholipids. *Biochemistry*. 51:3170–3177. <https://doi.org/10.1021/bi300086c>